JOURNAL OF DEFENCE AND SECURITY INDUSTRY

Journal of Defence and Security Industries: Strategy and Technology, 2026, 1(2)

Science & Technology Section

Design and Experimental Validation of an EMI Filter for Military DC-DC Converters Achieving MIL-STD-461G CE102 Compliance

İsmail Ovalı [1,*], İres İskender[2]

Abstract

This paper presents the design, implementation, and experimental validation of a practical Electromagnetic Interference (EMI) filter developed for military DC-DC converter applications in order to satisfy the conducted emission limits defined by MIL-STD-461G CE102. High-frequency switching behaviour, fast voltage and current transitions, and unavoidable parasitic elements in DC-DC converters make compliance with these limits extremely challenging without dedicated filtering, while practical military platforms impose severe constraints on size, stability, and realizability. In this paper, a systematic and iterative design methodology based on established EMI filter design principles is proposed, and the resulting attenuation performance is experimentally validated through CE102 measurements. The procedure includes determination of the design resistance considering the negative incremental impedance of the converter, design of Differential-Mode (DM) and Common-Mode (CM) stages, and suppression of resonance through properly selected damping networks. The resulting filter is implemented using commercially available components on a compact Printed Circuit Board (PCB) compatible with practical military installations. The performance of the proposed filter is verified experimentally through CE102 measurements performed under identical operating conditions for both filtered and unfiltered cases. The unfiltered converter is shown to exceed the CE102 limits, whereas the filtered configuration achieves compliance with sufficient margin across the entire frequency range. In addition, frequency-domain attenuation characteristics are measured using a Bode analyser to reveal the insertion loss behaviour of the filter. The consistency between analytical expectations, attenuation measurements, and compliance tests demonstrates that the proposed approach provides a reliable, repeatable, and application-oriented framework for EMI filter design in military power electronic systems.

Keywords: EMI, EMI filter, DC-DC converter, MIL-STD-461G CE102, insertion loss.

Received: 19.02.2026 Accepted: 22.05.2026 Research Article

[1] OB Sensor Technologies, Ankara, Türkiye
[2] Çankaya University, Ankara, Türkiye
* Corresponding author.
✉ ovaliiismail@gmail.com

Cite this article as:
https://doi.org/10.65834/jdsi.12.64
Ovalı, İ., & İskender, İ. (2026). Design and Experimental Validation of an EMI Filter for Military DC-DC Converters Achieving MIL-STD-461G CE102 Compliance. *Journal of Defence and Security Industries: Strategy and Technology 1(2)*, 157-176.

1. Introduction

Military electronic systems are required to operate reliably under stringent Electromagnetic Compatibility (EMC) constraints due to dense integration, harsh operating environments, and mission-critical functionality. Power electronic converters used in such platforms are among the primary sources of conducted Electromagnetic Interference (EMI), which may propagate through power lines and adversely affect neighbouring subsystems (Williams, 2001). To ensure compatibility, military standards impose strict emission limits; among them, MIL-STD-461G defines the CE102 requirement for power line conducted emissions over a wide frequency range (U.S. Department of Defence, 2015).

Modern DC-DC converters inherently generate significant conducted EMI due to high switching frequencies, fast voltage and current transitions, and unavoidable parasitic elements (Hartal, 1995). In practical military applications, compliance with CE102 limits is rarely achievable without dedicated EMI filtering. However, EMI filter design remains challenging because attenuation requirements must be satisfied while preserving system stability, minimizing volume, and maintaining practical realizability.

In the recent power electronics literature, there is a significant shift toward Active EMI Filters (AEFs) and Hybrid EMI Filters (HEFs) to address the volumetric constraints of passive components. Fishta and Fiori (2026) utilized active capacitors to achieve a 50% reduction in magnetic volume for traction inverters, while Tian et al. (2026) proposed cascaded active structures to enhance CM attenuation for wide-bandgap drives. Although these methodologies offer substantial miniaturization, they introduce significant control complexity, require auxiliary power supplies, and are subject to bandwidth limitations imposed by the gain-bandwidth product of operational amplifiers, often leading to performance degradation above 3 MHz. For mission-critical military platforms, where extreme reliability, structural simplicity, and robust performance under harsh environments are paramount, passive EMI filters remain the preferred and most reliable solution.

However, existing passive EMI filter design procedures in the literature often exhibit specific limitations in practical military applications, particularly regarding size, high-frequency performance, and system stability. Traditional approaches, such as those detailed by Cadirci et al. (2005) and Kichouliya et al. (2023), primarily rely on baseline noise measurements to determine the required insertion loss. While effective for their specific setups, this strictly attenuation-driven approach often leads to sub-optimal designs. For example, to meet a 60 dB low-frequency attenuation target, Kichouliya et al. (2023) employed disproportionately large magnetic components, requiring a massive 21.1 mH CM choke. In contrast, the proposed methodology in this study achieves a superior CM attenuation of 75 dB at 500 kHz using a significantly smaller 390 μH choke. Furthermore, conventional filters often suffer from high-frequency degradation; Cadirci et al. (2005) reported significant performance loss and limit violations above 5 MHz due to the unsuppressed self-resonances of the filter components. By deliberately incorporating RC damping networks, the proposed design effectively suppresses these high-Q resonances, maintaining robust attenuation across the entire CE102 frequency spectrum.

Beyond physical size and resonance issues, many existing studies focus on achieving theoretical insertion loss but completely neglect the dynamic stability of the overall system. Specifically, the interaction between the EMI filter's output impedance and the DC-DC converter's negative incremental input resistance (R_n) is frequently overlooked in classical designs. Ignoring this impedance interaction can lead to unforeseen oscillations and severe system instability under varying load conditions. The proposed methodology addresses this critical gap by integrating the converter's R_n into the core of the design process. By establishing a design resistance (R_d) that is strictly smaller than the magnitude of the negative input resistance $(R_d \leq |R_n|)$, the proposed framework guarantees robust stability while simultaneously optimizing the component values. This stability-oriented approach ensures that the filter not only meets stringent military emission limits but also preserves the reliable operation of the converter.

To address these gaps, this study proposes a systematic and iterative passive design methodology that prioritizes both compliance and system stability. Unlike previous works that rely on oversized inductors, the proposed framework integrates the determination of a design resistance (R_d) based on the converter's negative incremental input resistance (R_n) to guarantee robust dynamic stability. Furthermore, it utilizes RC damping networks to suppress high-Q resonances, optimizing the CM and DM stages to achieve superior attenuation. This structured design flow allows for the realization of the filter using compact, Commercially Available Off-The-Shelf (COTS) components within a size envelope suitable for military platforms. In order to define realistic design targets, publicly available datasheet information of representative military-grade DC-DC converters and their associated EMI filters was reviewed. Observations indicating that dominant emissions typically concentrate around switching frequencies near 250 kHz and their harmonics guided the identification of the most critical emission frequencies.

In this study, by bridging the gap between theoretical filter principles and the practical constraints of military DC-DC converters, the effectiveness of the proposed filter is evaluated through both simulation and rigorous experimental investigations. Conducted emission measurements are performed according to the MIL-STD-461G CE102 setup under realistic operating conditions to assess compliance. In addition, frequency-domain insertion loss characteristics are obtained using a Bode analyser, enabling a detailed physical observation of the filter's attenuation behaviour.

The primary contributions of this study are summarized as follows:

- A systematic and practical EMI filter design methodology tailored to MIL-STD-461G CE102 requirements, explicitly incorporating dynamic stability (R_n) and resonance damping.

- Comprehensive experimental characterization of the filter's attenuation capability through both standard CE102 compliance measurements and Bode analyser-based frequency response analysis.
- Demonstration of direct applicability to real military systems through a size-constrained hardware implementation and successful validation on a high-frequency DC-DC converter.

2. Design Methodology

This section presents the proposed EMI filter design methodology for a military DC-DC converter targeting compliance with the MIL-STD-461G CE102 conducted emission limits. The procedure follows a systematic and iterative framework derived from established EMI filter design principles (Nave, 1991; Ozenbaugh & Pullen, 2012) while accounting for practical implementation constraints.

To establish realistic design expectations, publicly available datasheet information from representative military-grade DC-DC converters and EMI filters was reviewed. This reference provides practical guidance regarding dominant frequency regions and achievable attenuation levels.

2.1. Background on EMC and MIL-STD-461G CE102

EMC is defined as the ability of an electronic system to function correctly in its electromagnetic environment without introducing intolerable EMI to other equipment. In Switch-Mode Power Supplies (SMPS) like military DC-DC converters, EMI is inherently generated by the high dv/dt and di/dt characteristics of semiconductor switching actions. This noise propagates through conduction along power lines (conducted emissions) or through radiation (radiated emissions).

To ensure reliable operation in dense military platforms, the MIL-STD-461G standard establishes strict testing procedures and emission limits. Specifically, the CE102 requirement evaluates conducted emissions on power leads within the frequency range of 10 kHz to 10 MHz. The measurement methodology requires the use of Line Impedance Stabilization Networks (LISNs), typically standardized at 50 µH, placed between the power source and the Equipment Under Test (EUT). The LISNs serve a dual purpose: they provide a defined, stable Radio-Frequency (RF) impedance to the EUT across the measurement band, and they isolate the test setup from ambient noise present on the facility's power grid. Compliance with CE102 guarantees that the high-frequency switching noise of the DC-DC converter will not degrade the performance of adjacent sensitive military electronics sharing the same power distribution bus.

2.2. Design Methodology Overview

The proposed approach consists of the following sequential steps:

- Determination of the design resistance from converter input characteristics,
- Design of the DM filter,
- Suppression of DM resonances through damping networks,
- Design of the CM filter,
- Suppression of CM resonances, and
- Integration and simulation-based verification of the EMI filter design.

This structured process enables predictable attenuation performance while maintaining system stability and realizability.

2.3. Determination of Design Resistance

Switch-mode DC-DC converters exhibit a negative incremental input impedance due to constant power behaviour. It can be approximated as

$$R_n = -\left|\frac{V_{in}}{I_{in}}\right| \quad (1)$$

where V_{in} and I_{in} denote the input voltage and current.

For stable interaction, the output impedance of the EMI filter must remain significantly smaller than the magnitude of the converter input impedance (Middlebrook, 1976):

$$|Z_o| \leq |R_n| \quad (2)$$

Since the filter design resistance R_d equals the filter's output impedance Z_o at a quality factor $Q = 1$, R_d must be chosen to be smaller than the magnitude of the negative incremental input resistance, $|R_n|$.

$$R_d \leq |R_n| \quad (3)$$

To obtain a realistic reference, a representative military-grade DC-DC converter was considered. Based on publicly available datasheet specifications of SynQor MCOTS-C-28VE-05-QT (SynQor, 2016), the converter operates over an input voltage range of 9-70 V with a rated output power of 85 W. The worst-case condition in terms of minimum input impedance occurs at the lowest input voltage, where the input current reaches its maximum value. Using this operating point and accounting for the converter's rated efficiency of 86%, the maximum input power is approximately 98.8 W. This yields a minimum negative input resistance magnitude ($|R_n|$) of approximately 0.82 Ω.

For the proposed filter, $R_d = 0.3\ \Omega$ is adopted, which corresponds to approximately 36% of the minimum calculated $|R_n|$. This ratio ensures that the filter's output impedance remains well below the converter's input impedance, providing sufficient margin against instability while also helping to limit excessive resonance within the filter network.

2.4. DM Filter Design

When selecting the filter topology, L, T, and π-type configurations are the primary candidates. An L-type filter is a second-order network providing an attenuation slope of 40 dB/decade, which is insufficient to meet the stringent high-frequency attenuation targets of military applications. Both T and π-type filters are third-order networks offering a steeper 60 dB/decade roll-off. However, a T-type filter presents a high inductive impedance to the converter, which can cause excessive voltage spikes when interacting with the pulsed input current of switch-mode DC-DC converters. Therefore, a π-type filter topology is selected for the DM stage; its capacitive output provides a low-impedance path for high-frequency switching currents while achieving the required 60 dB/decade attenuation slope (Tarateeraseth, 2011, 2012a, 2012b). The attenuation requirement is defined with respect to the dominant emission band identified for the targeted application.

The cut-off frequency of the DM filter is derived from the attenuation objective according to

$$f_{CDM} = \frac{f_{DM}}{\sqrt[6]{64 \times \left(10^{\frac{Att_{DM}}{10}} - 1\right)}} \tag{4}$$

where f_{DM} denotes the frequency of interest and Att_{DM} represents the desired attenuation level.

As observed in the baseline measurements (detailed in Section 3), the unfiltered system initially exceeds the CE102 limit at the converter's switching frequency of 83 kHz by approximately 25 dB. Although the minimum required attenuation could be derived directly from these unfiltered noise levels, merely targeting such relatively low attenuation values may not provide sufficient margin against the rigorous demands of military applications. To establish a more realistic and robust target, the performance levels of military-grade EMI filters were considered. According to the publicly available datasheet of the SynQor MCOTS-F-28-P-DM, DM attenuation values on the order of 80 dB are specified around 500 kHz (SynQor, 2024). Consequently, this information was adopted as a practical benchmark, and the DM attenuation target for the proposed design was selected as 80 dB at 500 kHz.

Using $f_{DM} = 500\ kHz$ and $Att_{DM} = 80\ dB$, the theoretical cut-off frequency becomes

$$f_{CDM} = \frac{500k}{\sqrt[6]{64 \times \left(10^{\frac{80}{10}} - 1\right)}} \cong 11.6\ kHz \tag{5}$$

To accommodate parasitic elements, component tolerances, and modelling uncertainties, the practical cut-off frequency is conservatively selected below the theoretical estimate.

Once the cut-off frequency is defined, the total inductance and capacitance values are calculated from the design resistance as

$$L_t = \frac{R_d}{2 \times \pi \times f_{CDM}} \tag{6}$$

$$C_t = \frac{1}{2 \times \pi \times R_d \times f_{CDM}} \tag{7}$$

Using $R_d = 0.3\ \Omega$ and a practical cut-off frequency of 10 kHz, the resulting component values are

$$L_t = 4.77\ \mu H \quad (8)$$
$$C_t = 53.05\ \mu F \quad (9)$$

Finally, the nearest standard component ratings are selected to enable practical hardware implementation.

2.5. DM Damping Design

High quality-factor resonances may deteriorate attenuation performance and destabilize the interaction between the converter and the EMI filter. To mitigate this effect, RC shunt damping branches are connected across the DM capacitors.

The damping resistance is selected equal to the design resistance,

$$R_{DD} = R_d \quad (10)$$

which ensured adequate energy dissipation once the damping network becomes active.

The damping capacitance is chosen such that the resistive action is effectively introduced in the vicinity of the resonance frequency while minimizing additional losses outside this band. In practical EMI filter implementations, empirical design heuristics are frequently employed to guarantee robust behaviour. A widely adopted approach is to select the damping capacitance several times larger than the main DM capacitor.

In the present design, a factor of approximately four is used. This choice enables strong resonance suppression without significantly affecting low-frequency operation or increasing unnecessary power dissipation.

2.6. CM Filter Design

Similar to the DM stage, the topology of the CM filter must be carefully selected to provide sufficient attenuation slope. To achieve a steep attenuation roll-off of approximately 60 dB/decade at high frequencies, a third-order π-type structure composed of a CM choke and two sets of Y-capacitors is implemented. This configuration provides superior high-frequency suppression compared to a standard 40 dB/decade L-type CM filter. In practical military applications, however, safety and leakage current regulations impose strict limits on the total Y-capacitance connected to chassis ground. These constraints directly influence achievable cut-off frequencies and CM choke values. The attenuation objective is defined with respect to the dominant emission region identified for the application.

Similar to the DM design, to establish a realistic target, performance levels of military-grade EMI filters are considered. According to publicly available datasheet information of SynQor MCOTS-F-28-P-DM, CM attenuation values on the order of 60 dB are specified around 500 kHz (SynQor, 2024). This information is therefore adopted as a practical benchmark for the proposed design.

The cut-off frequency is calculated from the attenuation requirement as

$$f_{CCM} = \frac{f_{CM}}{\sqrt[6]{64 \times \left(10^{\frac{Att_{CM}}{10}} - 1\right)}} \tag{11}$$

Using $f_{CM} = 500\ kHz$ and $Att_{CM} = 60\ dB$, the theoretical cut-off frequency becomes

$$f_{CCM} \cong 25\ kHz \tag{12}$$

Due to safety and leakage current limitations, the total allowable Y-capacitance is restricted. In the present design, the aggregate value is selected as

$$C_y = 0.60\ \mu F \tag{13}$$

Based on the selected cut-off frequency of 15 kHz and total Y-capacitance, the required CM inductance is obtained as

$$L_{CM} = \frac{1}{2 \times \pi^2 \times {f_{CCM}}^2 \times C_y} \tag{14}$$

which yields approximately

$$L_{CM} \cong 375\ \mu H \tag{15}$$

For practical implementation, the nearest standard value of 390 µH is selected.

It should be noted that the physical implementation of the CM choke introduces a leakage inductance, which appears in series with the DM path. As discussed later in Section 4, this leakage inductance inherently contributes to the total DM inductance, lowering the effective cut-off frequency and enhancing low-frequency DM attenuation. However, to maintain a conservative design, this added additional attenuation is not factored into the initial ideal calculations.

2.7. CM Damping Design

To suppress high-Q resonance behaviour in the CM network, an RC damping branch is introduced. A practical and widely used approach is to select the damping resistance close to the characteristic impedance of the CM filter.

Accordingly, the damping resistance is approximated as

$$R_{CD} = \sqrt{\frac{2 \times L_{CM}}{C_y}} \tag{16}$$

Using $L_{CM} = 390\ \mu H$ and $C_y = 0.60\ \mu F$, the resulting value becomes

$$R_{CD} \cong 36\ \Omega \tag{17}$$

The damping capacitance is then chosen such that the resistive damping action becomes effective around the resonance frequency while minimizing additional losses outside the targeted band.

2.8. Integration and Simulation-Based Design Verification

The DM and CM sections are combined into a unified EMI filter structure in order to evaluate overall response prior to hardware realization. The complete circuit is implemented in LTspice using the component values obtained in the previous subsections.

Figure 1 illustrates the DM, CM, and integrated filters modelled in LTspice for the simulation. The simulated DM attenuation is presented in Figure 2. The response indicates strong suppression in the dominant emission region while maintaining a smooth transition toward lower frequencies. No excessive resonance amplification is observed, confirming the effectiveness of the damping strategy.

Similarly, the CM attenuation characteristic is given in Figure 3. The results demonstrate that the CM stage provides the intended reduction across the targeted frequency band and that high-Q behaviour is effectively controlled.

At 500 kHz, the simulated attenuation reaches approximately 156.09 dB for the DM case and 94.80 dB for the CM case. These values correspond to idealized simulation conditions in which parasitic couplings, layout effects, and non-ideal component characteristics are not fully represented. Consequently, lower attenuation levels are expected in practical hardware realization (Chiu et al., 2024; Wang et al., 2004). Nevertheless, the simulation results clearly indicate that sufficient design margin exists with respect to the targeted attenuation requirements.

Overall, the simulation study confirms that the selected parameters are appropriate for meeting the intended attenuation objectives before proceeding to experimental validation. Hardware-based conducted emissions measurements are provided in the following section.

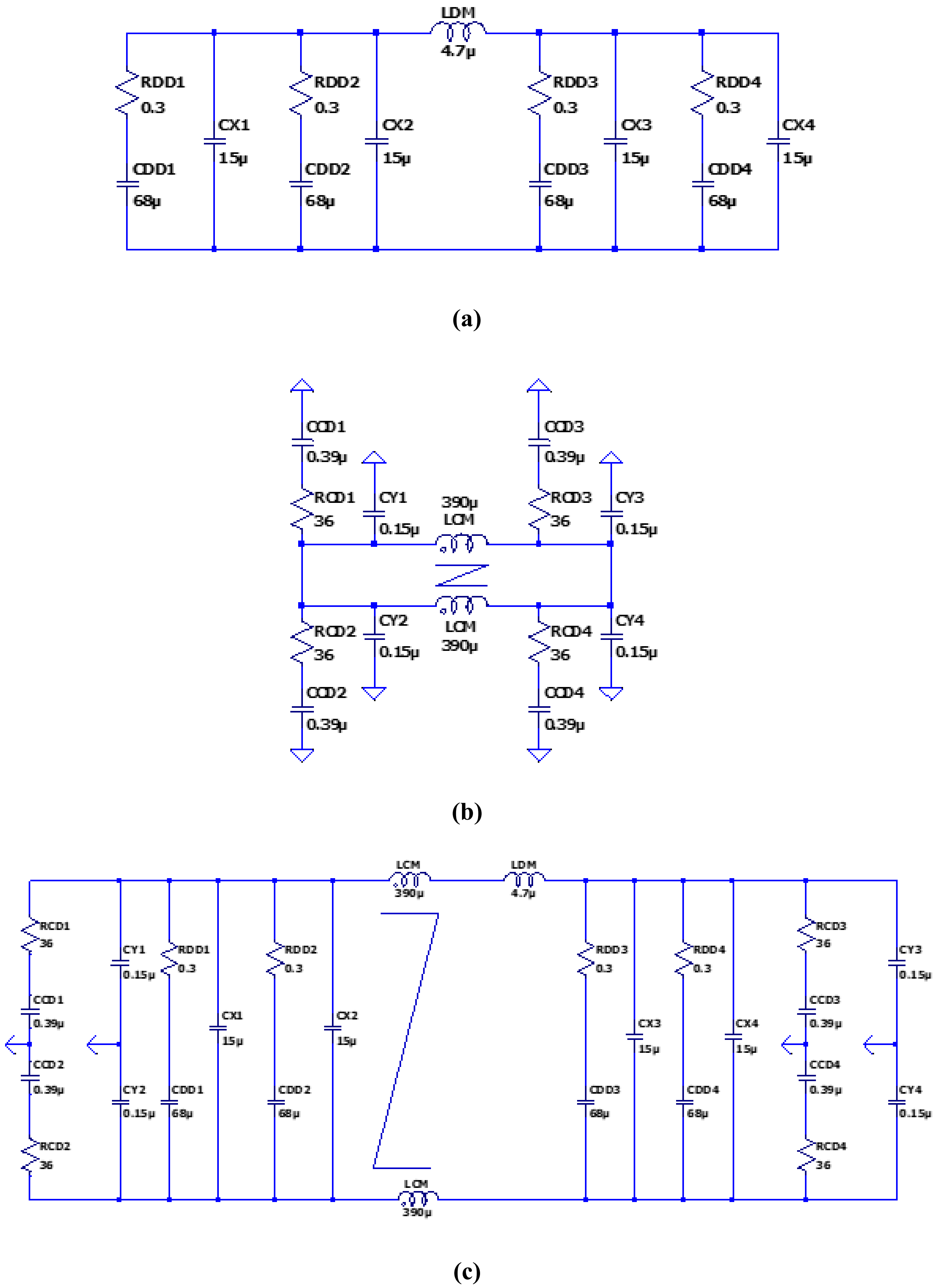

Figure 1. Filters modelled in LTspice for simulation: **(a)** DM filter, **(b)** CM filter, and **(c)** integrated filter.

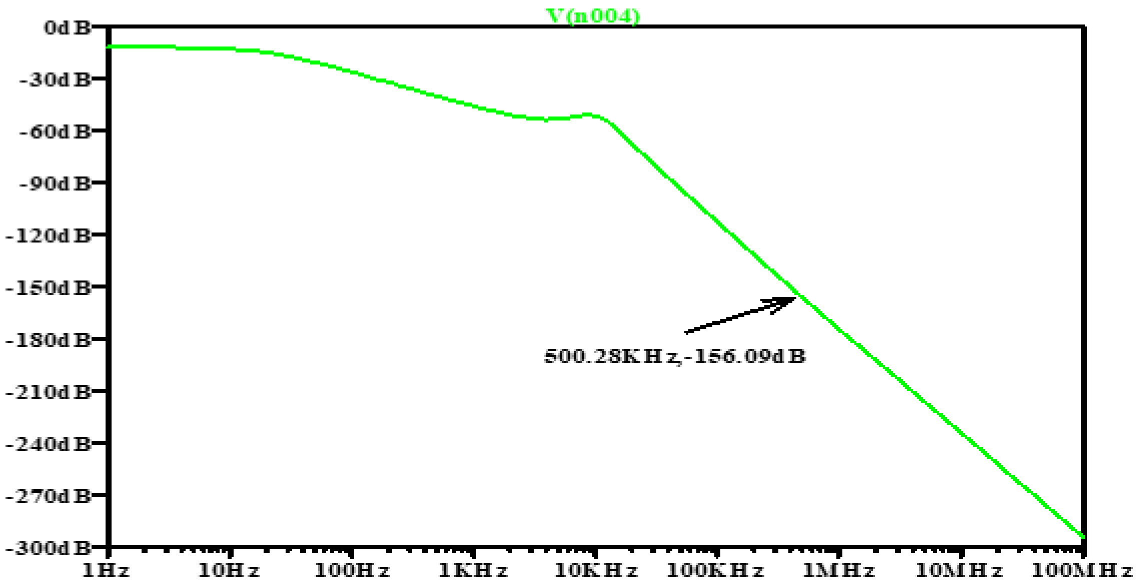

Figure 2. Simulated DM attenuation of the proposed EMI filter obtained from the integrated LTspice model.

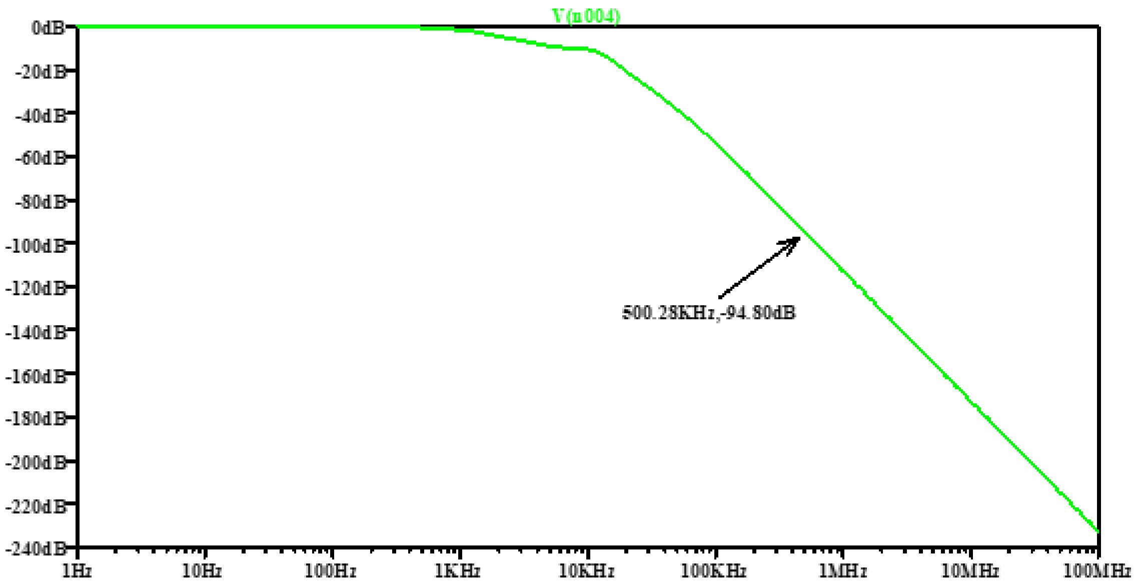

Figure 3. Simulated CM attenuation of the proposed EMI filter obtained from the integrated LTspice model.

3. Results

This section presents the experimental evaluation of the proposed EMI filter and demonstrates its effectiveness under realistic operating conditions. The validation is performed through conducted emissions measurements according to the CE102 requirement and complementary frequency-domain insertion loss analysis. Together, these tests provide verification of both standard compliance and the underlying attenuation mechanisms.

The EMI filter is realized using commercially available components and assembled on a dedicated printed circuit board. The prototype is designed with clear separation between CM and DM sections, while damping networks are integrated to suppress resonance phenomena. The compact implementation confirms that the proposed methodology leads to a solution compatible with practical military integration constraints.

The fabricated prototype is shown in Figure 4(a) and Figure 4(b), illustrating the top and bottom views of the board, respectively.

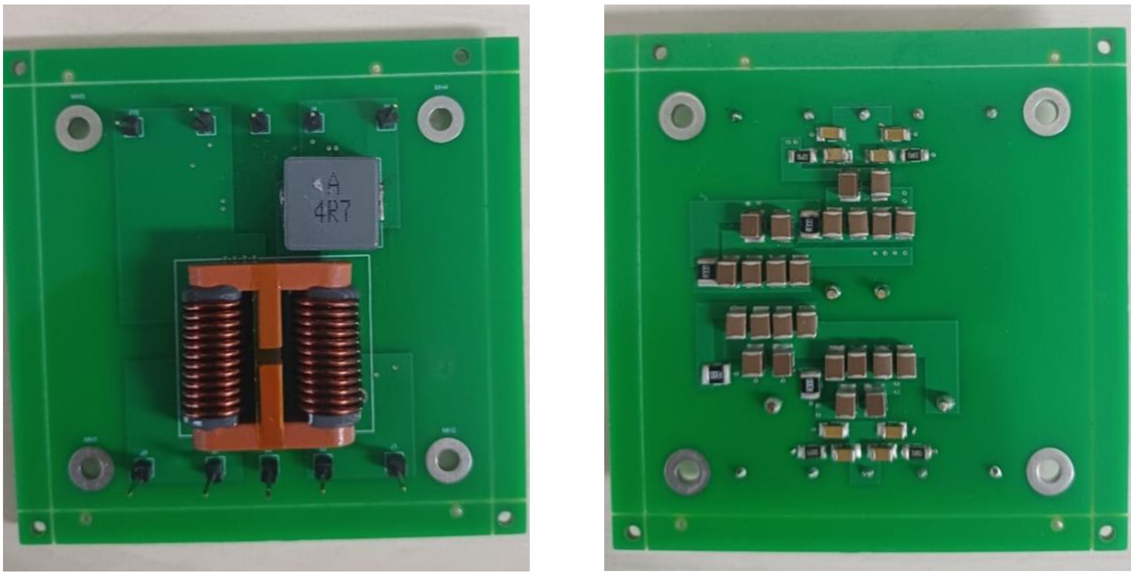

(a) (b)

Figure 4. EMI filter prototype: **(a)** top view and **(b)** bottom view.

Following prototype realization, conducted emissions tests and frequency-domain measurements are carried out. The corresponding results are detailed in the subsequent subsections.

3.1. CE102 Conducted Emission Results

Conducted emission measurements are performed to experimentally verify compliance with the CE102 requirement. The test configuration is illustrated in Figure 5. Figure 5(a) shows the baseline setup without the EMI filter, while Figure 5(b) presents the configuration with the proposed filter inserted at the converter input. The DC–DC converter is powered through LISNs), and the conducted noise is measured separately on the positive and negative input lines. All tests are conducted under identical input voltage and load conditions to enable a fair comparison between filtered and unfiltered operation.

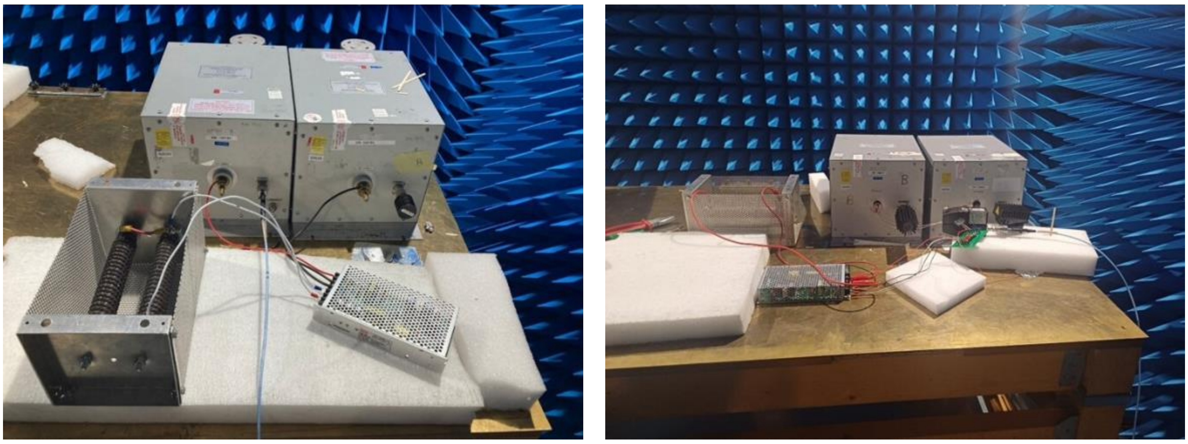

(a) **(b)**

Figure 5. CE102 test configuration: **(a)** without EMI filter and **(b)** with the proposed EMI filter.

The baseline results obtained without the EMI filter are presented in Figure 6(a) and Figure 6(b) for the positive and negative lines, respectively. The spectra clearly exceed the CE102 limits; specifically, the first significant violation occurs at the converter's switching frequency of 83 kHz, where the emissions exceed the limit by approximately 25 dB. These observations confirm that additional filtering is mandatory for standard compliance.

Following integration of the proposed EMI filter, the measurements are repeated. The corresponding results are shown in Figure 7(a) and Figure 7(b). A substantial reduction in conducted noise is observed across the entire frequency range. The emission levels remain below the CE102 limits with visible margin for both lines, demonstrating successful mitigation of interference.

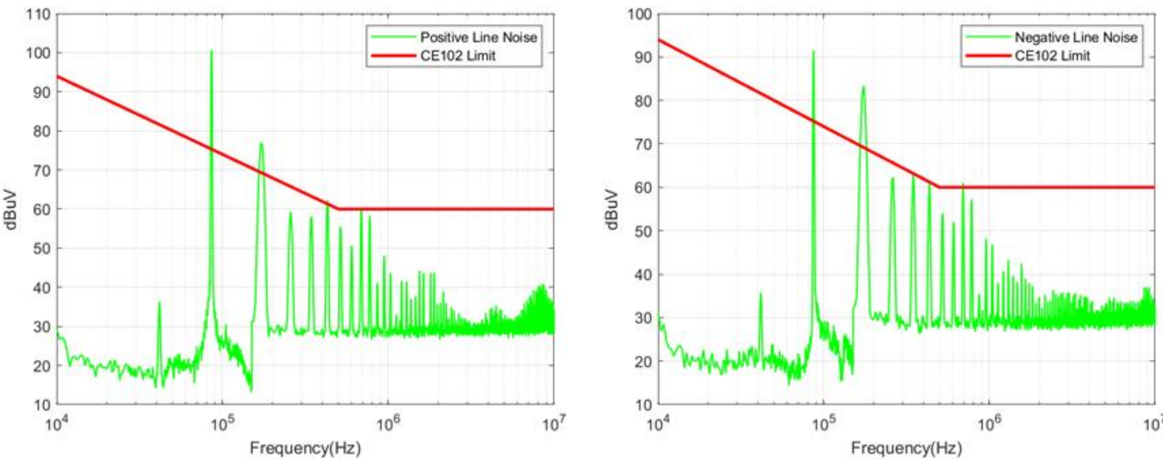

(a) **(b)**

Figure 6. Baseline CE102 conducted emission results without the EMI filter: **(a)** positive line and **(b)** negative line.

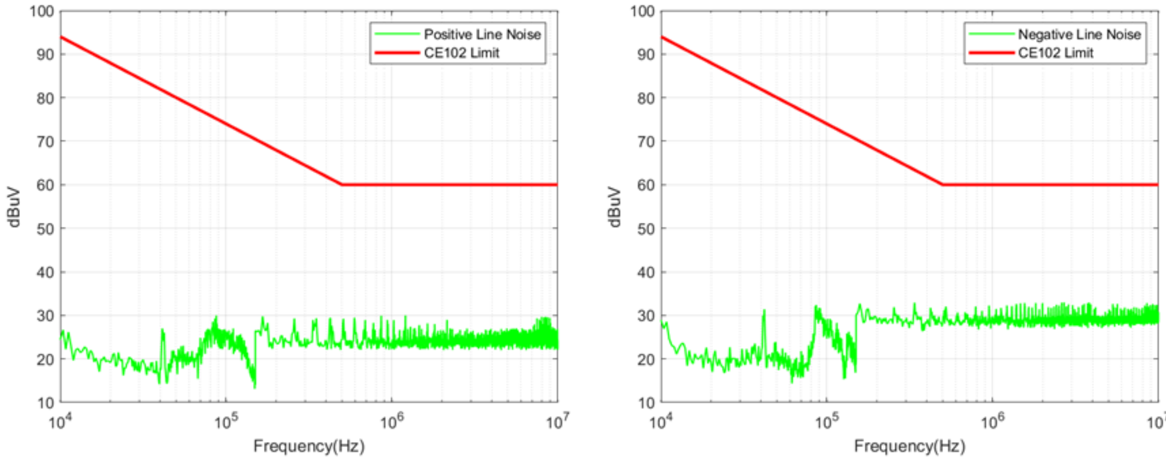

(a) **(b)**

Figure 7. CE102 conducted emission results with the proposed EMI filter: **(a)** positive line and **(b)** negative line.

Moreover, the close similarity between the positive and negative line responses indicates symmetrical and consistent filter behaviour, further validating the robustness of the design.

3.2. Frequency-Domain Insertion Loss Results

While CE102 testing provides direct confirmation of standard compliance, it does not fully reveal how attenuation is distributed across frequency or how the CM and DM sections contribute to the overall performance. For this reason, insertion loss measurements are performed using a Bode analyser.

The measured CM insertion loss is presented in Figure 8 and Figure 9 for the low and high-frequency ranges, respectively. In the lower frequency region, the experimental results generally follow the trend predicted by simulations, and the filter exhibits the expected attenuation behaviour. Around 500 kHz, approximately 75 dB attenuation is obtained, exceeding the initial 60 dB objective.

At higher frequencies, however, the attenuation deviates from the ideal response and decreases to nearly 55 dB in certain regions. These variations are primarily attributed to non-ideal effects such as parasitic capacitances, leakage paths, component self-resonances, and layout-related couplings. Such mechanisms become dominant in the MHz range and limit the achievable performance compared to ideal simulations.

The DM insertion loss is shown in Figure 10 and Figure 11. In the low-frequency region, the measured attenuation is notably higher than predicted by simulations, indicating that the effective filtering action begins earlier than anticipated during the design stage. This behaviour is mainly associated with additional parasitic inductive contributions that are not fully captured in the idealized model.

At 500 kHz, the measured attenuation is approximately 55 dB, which is lower than the 80 dB benchmark adopted during design. Furthermore, the attenuation profile is not strictly monotonic across frequency; depending on resonance interactions, local improvements or degradations are observed. Such deviations from ideal predictions are expected in practical implementations due to parasitic couplings, leakage inductances, component self-resonance, PCB layout effects, and measurement fixture influences.

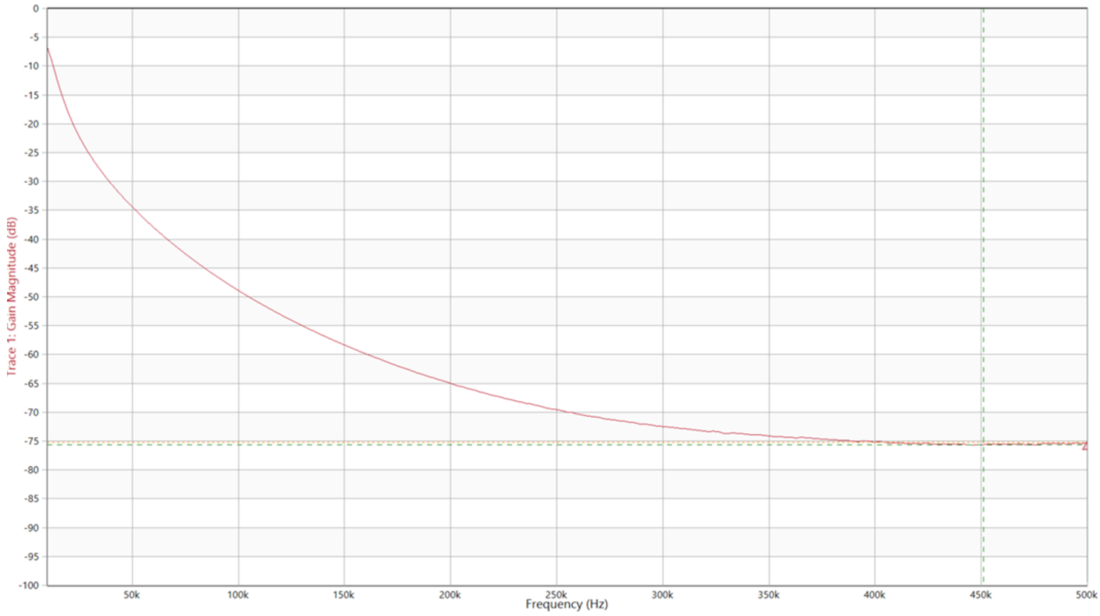

Figure 8. Measured CM insertion loss in the 0-500 kHz frequency range.

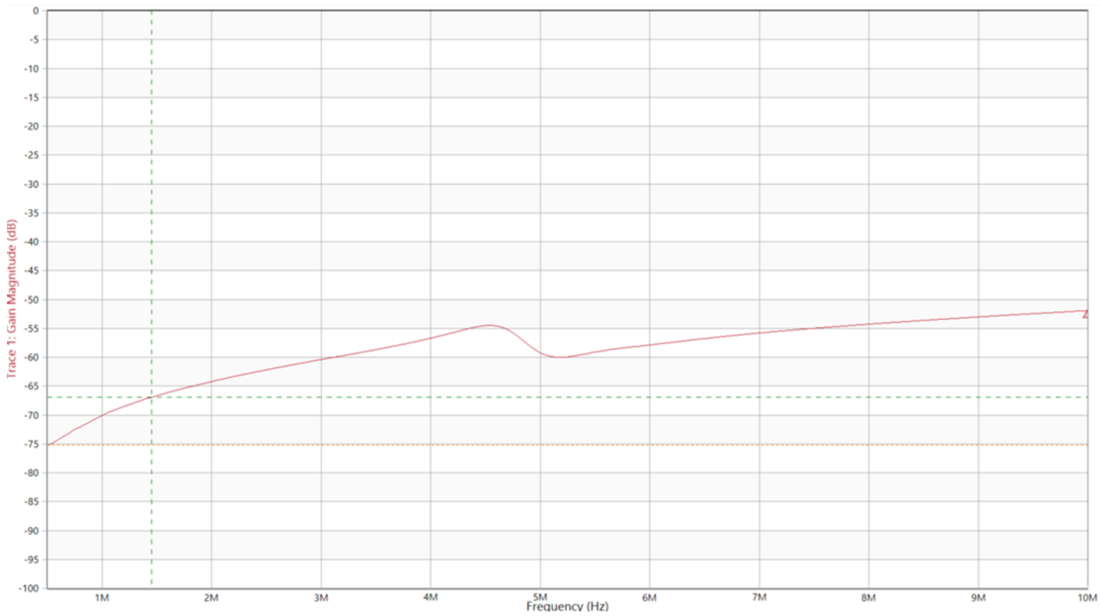

Figure 9. Measured CM insertion loss in the 500 kHz-10 MHz frequency range.

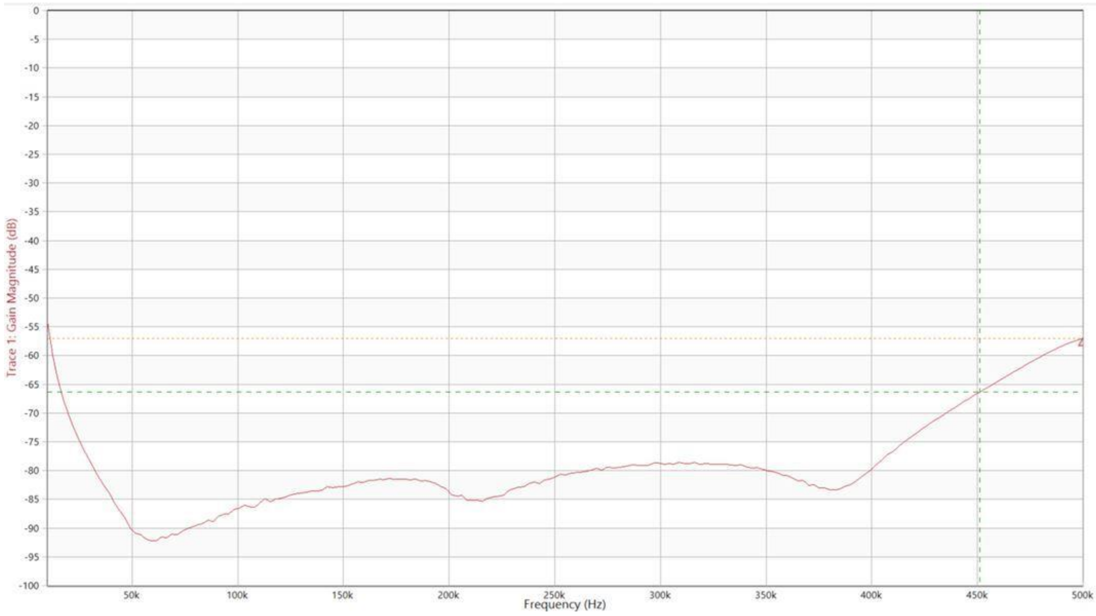

Figure 10. Measured DM insertion loss in the 0-500 kHz frequency range.

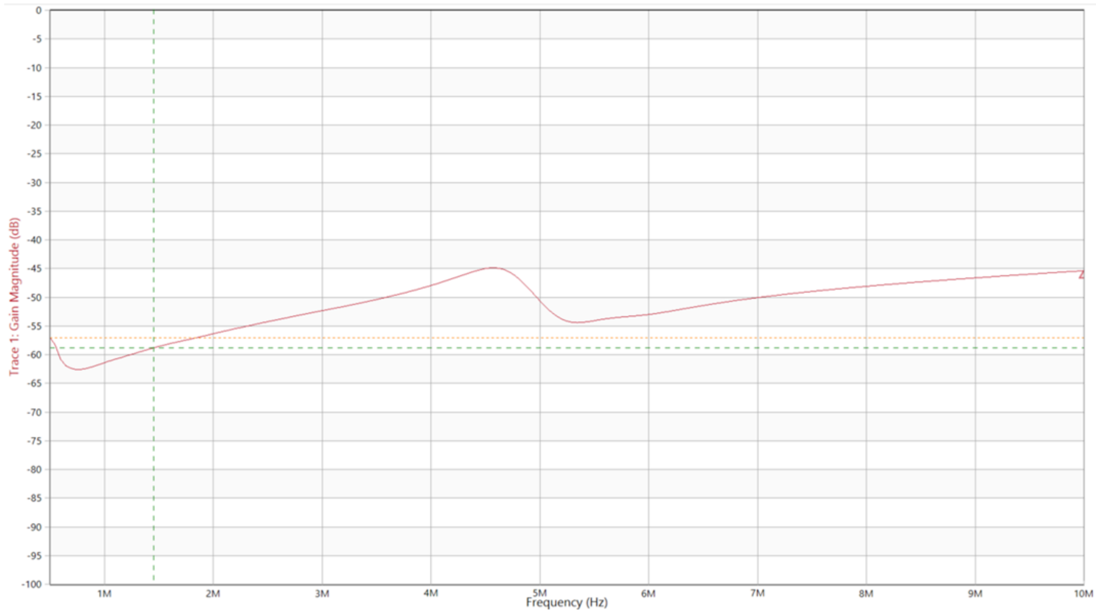

Figure 11. Measured DM insertion loss in the 500 kHz-10 MHz frequency range.

Despite these deviations, the measurements confirm that substantial suppression is achieved within the frequency region critical for CE102 compliance. The presence of frequency-dependent variations further highlights the importance of parasitic and cross-coupling effects, which are investigated in more detail in the Discussion section.

Overall, the Bode analyser results provide physical interpretation of the successful CE102 performance and demonstrate that the realized filter maintains effective attenuation even under non-ideal practical conditions.

4. Discussion

The experimental and frequency-domain results provide valuable insight into the practical behaviour of the proposed EMI filter, highlighting both the differences between idealized predictions and real hardware performance, as well as its advantages over existing methodologies in the literature.

One of the most notable observations is the variation between simulation and measurement outcomes. In the low-frequency region, the measured attenuation, particularly in DM, is in several cases higher than predicted. This indicates that additional inductive contributions, such as leakage inductance from the CM choke and unintended parasitic elements, effectively shift the filter action toward lower frequencies.

In contrast, as frequency increases, the measured attenuation becomes limited compared to simulation expectations. The reduction in performance is primarily associated with parasitic capacitances, component self-resonances, and coupling mechanisms introduced by the physical implementation. These effects create alternative propagation paths and resonance conditions that cannot be fully captured in ideal circuit representations.

A dominant contributor to the discrepancy between simulation and measurement is the leakage inductance of the CM choke. Experimental measurements show that this parasitic inductance (~15 μH) is several times larger than the nominal DM inductance assumed during the design stage. Consequently, the effective inductance in the DM path increases, shifting the cut-off frequency toward lower values. This mechanism explains the improved attenuation observed at low frequencies while simultaneously moving self-resonance and interaction effects into earlier regions of the spectrum, thereby constraining high-frequency performance. However, unlike the models proposed by Cadirci et al. (2005), which showed significant performance degradation above 5 MHz due to self-resonance effects, the filter in this study maintained effective attenuation across the entire CE102 spectrum due to optimized layout considerations and resonance suppression.

Beyond these physical insights, the results demonstrate a significant advantage of the proposed framework in achieving superior attenuation and volumetric efficiency through a stability-oriented design flow. For instance, while high-performance active designs such as the cascaded FF-FB AEF reported by Tian et al. (2026) achieved a CM attenuation of 42 dB, the passive filter in this study reached 75 dB at 500 kHz. Furthermore, conventional passive approaches, such as the one detailed by Kichouliya et al. (2023), often require very large magnetic components—such as 21.1 mH CM chokes—to meet low-frequency limits in high-power systems. By integrating the converter's negative incremental resistance into the determination of the design resistance and utilizing RC damping networks, this study achieves compliance with a significantly smaller 390 μH inductor. This demonstrates that prioritizing system stability allows for the use of larger capacitances and smaller inductances without compromising the compact physical envelope required for military platforms.

Despite the non-ideal limitations, both CE102 and Bode analyser measurements verify that the realized filter maintains sufficient attenuation in the frequency range critical for compliance. The existence of margin under realistic parasitic conditions confirms the robustness of the proposed design methodology. From an engineering standpoint, the findings emphasize that accurate prediction of high-frequency performance requires detailed modelling of parasitic elements, component construction, and PCB layout. Nevertheless, despite the added complexity of active alternatives, this study confirms that a systematic passive approach provides a more robust, reliable, and simpler framework that leads to successful MIL-STD-461G compliance without excessive redesign effort.

5. Conclusion

This paper presented a systematic and practical EMI filter design methodology for military DC–DC converter applications targeting compliance with the MIL-STD-461G CE102 conducted emission limits. The approach links attenuation objectives, stability considerations, and realizable component values within a structured design flow.

The proposed filter was implemented using commercially available components and validated through both CE102 measurements and frequency-domain insertion loss analysis. The experimental results demonstrated that, while deviations from ideal simulations arise due to parasitic effects and component non-idealities, sufficient attenuation margin is maintained within the frequency region critical for compliance. The agreement between analytical expectations, simulations, and hardware measurements confirms that the methodology provides a reliable and repeatable framework for practical EMI mitigation.

The study also highlighted the strong influence of parasitic elements, particularly the leakage inductance of the CM choke, on the overall filter behaviour. These findings underline the necessity of considering cross-coupling between CM and DM paths in real implementations.

Future work may focus on incorporating detailed parasitic models into early-stage simulations to improve prediction accuracy, especially in the high-frequency region. In addition, optimization of magnetic component design, including custom winding strategies for CM chokes, represents a promising direction for enhancing performance. Further research may also explore mechanical integration concepts that facilitate direct deployment of compact EMI filtering solutions in military and aerospace platforms, as well as the inclusion of extended protection features against abnormal operating conditions.

Funding

This research received no external funding.

Acknowledgments

The authors would like to thank Aselsan, Anova, and OB Sensör Teknolojileri for their support during the measurement and testing activities.

Ethical Statements

Not applicable.

Data and Code Availability

The data that support the findings of this study are available from the corresponding author upon reasonable request.

Supplementary Materials

Not applicable.

References

Cadirci, I., Saka, B., & Y. Eristiren. (2005). Practical EMI-filter-design procedure for high-power high-frequency SMPS according to MIL-STD 461. *IEE Proceedings*, 152(4), 775–775. https://doi.org/10.1049/ip-epa:20045079

Chiu, P.-T., Pong, M. H., Yao, C.-J., & Chiu, H.-J. (2024). The effect of parasitic elements on EMI common mode filter insertion loss. In *Proceedings of the International Conference on Industrial Electronics and Applications (ICIEA)* (pp. 1–6). https://doi.org/10.1109/ICIEA61579.2024.10664692

Fishta, M., & Fiori, F. (2026). A volume-optimized hybrid EMI filter for automotive traction inverters. *IEEE Transactions on Electromagnetic Compatibility*, 68(2), 321–329. https://doi.org/10.1109/TEMC.2026.3652665

Hartal, O. (1995). *EMC by design* (3rd ed.). R & B Enterprises.

Kichouliya, R., Sundar, S., & Reddy, P. (2023). Power line EMI filter design of power converters to meet the conducted emission specifications of MIL-STD-461G. In *Proceedings of the National Power Electronics Conference (NPEC)* (pp. 1–6). https://doi.org/10.1109/NPEC57805.2023.10385027

Middlebrook, R. D. (1976). Input filter considerations in design and applications of switching regulators. *Proc. IEEE IAS'76*, 91-107. https://ci.nii.ac.jp/naid/80014902952/

Nave, M. J. (1991). *Power line filter design for switched-mode power supplies.* Van Nostrand Reinhold.

Ozenbaugh, R. L., & Pullen, T. M. (2012). *EMI filter design* (3rd ed.). CRC Press.

SynQor. (2016). MCOTS-C-28VE-05-QT: Military COTS DC-DC Converter Datasheet. https://www.synqor.com/products/mil-cots/mcots-c-28ve-05-qt

SynQor. (2024). MCOTS-F-28E-P-DM: Military COTS EMI filter Datasheet. https://www.synqor.com/products/mil-cots/mcots-f-28e-p-dm

Tarateeraseth, V. (2011). EMI Filter Design Part I: Conducted EMI Generation Mechanism. In *IEEE Electromagn. Conf* (pp. 44-50).

Tarateeraseth, V. (2012a). EMI filter design part II: Measurement of noise source impedances. *IEEE EMC Magazine*, 1(1), 42–49. https://doi.org/10.1109/MEMC.2012.6244944

Tarateeraseth, V. (2012b). EMI filter design part III: Selection of filter topology for optimal performance. *IEEE EMC Magazine*, 1(2), 60–73. https://doi.org/10.1109/MEMC.2012.6244975

Tian, Y., Jiang, Y., Liao, Y., & Tan, Y. K. (2026). Highly-Efficient Cascaded Active EMI Filter for WBG-based integrated Motor Drive. *IEEE Journal of Emerging and Selected Topics in Power Electronics*, 1–1. https://doi.org/10.1109/jestpe.2026.3677211

U.S. Department of Defense. (2015). MIL-STD-461G: *Requirements for the control of EMI characteristics of subsystems and equipment*. U.S. Government Printing Office.

Wang, S., Lee, F. C., Chen, D. Y., & Odendaal, W. G. (2004). Effects of parasitic parameters on EMI filter performance. *IEEE Transactions on Power Electronics*, 19(3), 869–877. https://doi.org/10.1109/TPEL.2004.826527

Williams, T. (2001). *EMC for product designers* (3rd ed.). Newnes.